Bias field tunable magnetic configuration and magnetization dynamics in $Ni_{80}Fe_{20}$ nano-cross structures with varying arm length

K. Adhikari, S. Choudhury, R. Mandal, S. Barman, Y. Otani, and A. Barman

Citation: Journal of Applied Physics **121**, 043909 (2017);
View online: https://doi.org/10.1063/1.4974886
View Table of Contents: http://aip.scitation.org/toc/jap/121/4
Published by the American Institute of Physics

Bias field tunable magnetic configuration and magnetization dynamics in $Ni_{80}Fe_{20}$ nano-cross structures with varying arm length

K. Adhikari,[1] S. Choudhury,[1] R. Mandal,[1] S. Barman,[1] Y. Otani,[2,3] and A. Barman[1,a)]
[1]*Department of Condensed Matter Physics and Material Sciences, S. N. Bose National Centre for Basic Sciences, Block JD, Sector III, Salt Lake, Kolkata 700106, India*
[2]*CEMS-RIKEN, 2-1 Hirosawa, Wako, Saitama 351-0198, Japan*
[3]*Institute for Solid State Physics, University of Tokyo, 5-1-5 Kashiwanoha, Kashiwa, Chiba 277-8581, Japan*

(Received 1 October 2016; accepted 12 January 2017; published online 26 January 2017)

Ferromagnetic nano-cross structures promise exotic static magnetic configurations and very rich and tunable magnetization dynamics leading towards potential applications in magnetic logic and communication devices. Here, we report an experimental study of external magnetic field tunable static magnetic configurations and magnetization dynamics in $Ni_{80}Fe_{20}$ nano-cross structures with varying arm lengths (L). Broadband ferromagnetic resonance measurements showed a strong variation in the number of spin-wave (SW) modes and mode frequencies (f) with bias field magnitude (H). Simulated static magnetic configurations and SW mode profiles explain the rich variation of the SW spectra, including mode softening, mode crossover, mode splitting, and mode merging. Such variation of SW spectra is further modified by the size of the nano-cross. Remarkably, with decreasing arm length of nano-cross structures, the onion magnetization ground state becomes more stable. Calculated magnetostatic field distributions support the above observations and revealed the non-collective nature of the dynamics in closely packed nano-cross structures. The latter is useful for their possible applications in magnetic storage and memory devices. *Published by AIP Publishing.*
[http://dx.doi.org/10.1063/1.4974886]

I. INTRODUCTION

Recent attention in nanomagnetism[1,2] is triggered by their fundamental properties and huge potential applications in various fields of nanotechnology such as magnetic data storage,[2,3] logic devices,[4] waveguides,[5,6] filters,[7] phase shifters,[8] as well as spin torque nano-oscillators.[9] Emerging fields like magnonics[10,11] and magnon spintronics[12] promise on-chip data communication and processing, leading towards an all-magnetic computation. Future technology demands faster magnetic switching and spatial miniaturization. To design successful devices based on arrays of nanomagnets, it is crucial to understand their static and dynamic magnetic properties and to find means to control those by intrinsic and extrinsic parameters. To this end, significant efforts have been put towards understanding the dynamics of single nanomagnets[13–15] and arrays of nanomagnets.[16–23] The intrinsic magnetization dynamics of ferromagnetic nanodot arrays are primarily governed by nanodot size,[18,19] shape,[22] and areal density[21] and lattice symmetry[23] of the array. On the other hand, by varying the extrinsic parameters such as strength and orientation of the bias magnetic field, temperature, and spin transfer torque, the magnetization dynamics can be efficiently and directly controlled. The static magnetic configurations of the nanomagnet arrays play a crucial role in their magnetization dynamics and it may vary between single domain, quasi-single domain, closure domain, and multi-domain structures due to the interplay between the internal magnetic field, inter-element interaction field, and external bias field. Hence, by varying the above parameters, many static magnetic configurations and spin-wave (SW) properties, including SW frequency, damping, and spatial coherence, can be obtained.

Ferromagnetic cross-shaped elements showed complex spin configurations,[24] while the magnetization dynamics of $Ni_{80}Fe_{20}$ sub-micron cross arrays studied by a time-resolved magneto optical Kerr effect (TR-MOKE) microscope showed a strong configurational anisotropy.[25] A subsequent report[26] proposed application of ferromagnetic cross-shaped elements as reconfigurable spin-based logic devices using SW scattering and interference. The above results open a door for application of ferromagnetic cross structures as a building block of magnetic storage, memory, on-chip data communications, and spin-based logic devices, and hence, investigation of the static and dynamic magnetic properties of this structure with its size, inter-element interaction, and variation of the bias magnetic field has become important. Here, we report an extensive study of SW dynamics in $Ni_{80}Fe_{20}$ (Py) nano-crosses with varying arm lengths by using the broadband ferromagnetic resonance technique. We demonstrate the evolution of different types of magnetic configurations with bias magnetic field and the ensuing dynamical phenomena including a cross-over between SW modes, a minimum in the frequency spectra, and a mode splitting, which varied significantly with the size of the cross structure.

II. EXPERIMENTAL DETAILS

Arrays ($200\,\mu m \times 20\,\mu m$) of Py nano-crosses with the arm length (L) varying between 600 nm and 200 nm, fixed thickness (20 nm), and edge-to-edge separation (150 nm), as well as a continuous Py film of 20 nm thickness were

a)Email: abarman@bose.res.in

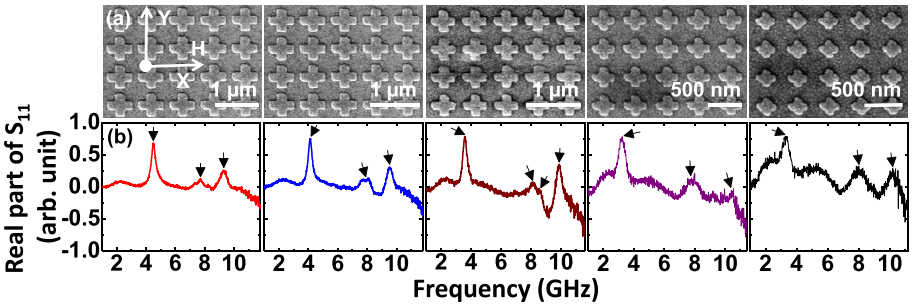

FIG. 1. (a) Scanning electron micrographs of $Ni_{80}Fe_{20}$ nano-cross arrays with varying arm lengths. The inset shows the applied magnetic field direction. (b) Real part of the S_{11} parameter as a function of frequency at H = 497 Oe for all samples. The SW modes are marked by arrows.

fabricated on a self-oxidized Si-substrate [001] by a combination of e-beam lithography and e-beam evaporation. The 20 nm thick Py film coated with a 60 nm thick Al_2O_3 protective layer was deposited in an ultra-high vacuum chamber at a base pressure of 2×10^{-8} Torr on a bi-layer (PMMA/MMA) resist pattern on the Si substrate made by using e-beam lithography. A Au made co-planer waveguide (CPW) of 150 nm thickness, 30 μm central conductor width, 300 μm length, and 50 Ω nominal characteristic impedance was deposited on top of the nano-cross structures and the continuous Py film at a base pressure of 6×10^{-7} Torr. Subsequently, a 5 nm thick Ti protective layer was deposited on top of the Au layer at the same base pressure. The waveguide was patterned by using mask-less photolithography. The FMR experiments were performed using a vector network analyzer (Agilent, PNA-L N5230C, 10 MHz to 50 GHz) and a homebuilt high frequency probe station with a non-magnetic G-S-G type probe (GGB Industries, Model No. 40 A-GSG-150-EDP).[27] A microwave signal with a power of −15 dBm and varying frequencies is applied to the CPW structure, and the output signal is collected from the CPW in the reflection geometry. A rotating electromagnet is used to apply an in-plane bias magnetic field up to 1.6 kOe. All the experiments are carried out at room temperature.

III. RESULTS AND DISCUSSION

Fig. 1(a) shows the scanning electron micrographs of all arrays while the bias magnetic field orientation is shown in the inset. The cross structures show rounded corners and edge deformations, which increases with the reduction of the cross size. The dimensions of the individual crosses and their separations in the arrays also vary by up to ±8%. Fig. 1(b) shows representative FMR spectra from the nano-cross structures, with the resonant peaks marked by arrows. There are some humps in the FMR spectra, which do not show any bias field dependence, and hence, considered of non-magnetic origin. The bias field dependent FMR spectra of the continuous Py film are also measured and the data are fitted using the Kittel formula to extract the material parameters, which are: saturation magnetization $M_S = 850$ emu/cc, gyromagnetic ratio $\gamma = 17.85$ MHz/Oe, and the anisotropy field $H_K = 0$. The bias field dependent FMR spectra for the Py nano-cross arrays with 200 nm ≤ L ≤ 600 nm are shown in Figs. 2(b)–2(f). All the nano-cross arrays show several SW modes, which depend on the bias field magnitude and the dimensions of the nano-cross structures. Some important features of the bias field dependence of the SW modes are as follows. (a) With the decrease in bias field, a crossover between the two lowest frequency branches is observed at an intermediate bias field value. This is followed by observation of a minimum, then one maximum, and a subsequent decrease in frequency with further reduction in the bias field of the lowest frequency branch. (b) A continuous decrease in frequency with the decrease in bias field for the intermediate frequency branch. (c) The frequency of two highest frequency branches decreases with bias field and merges to

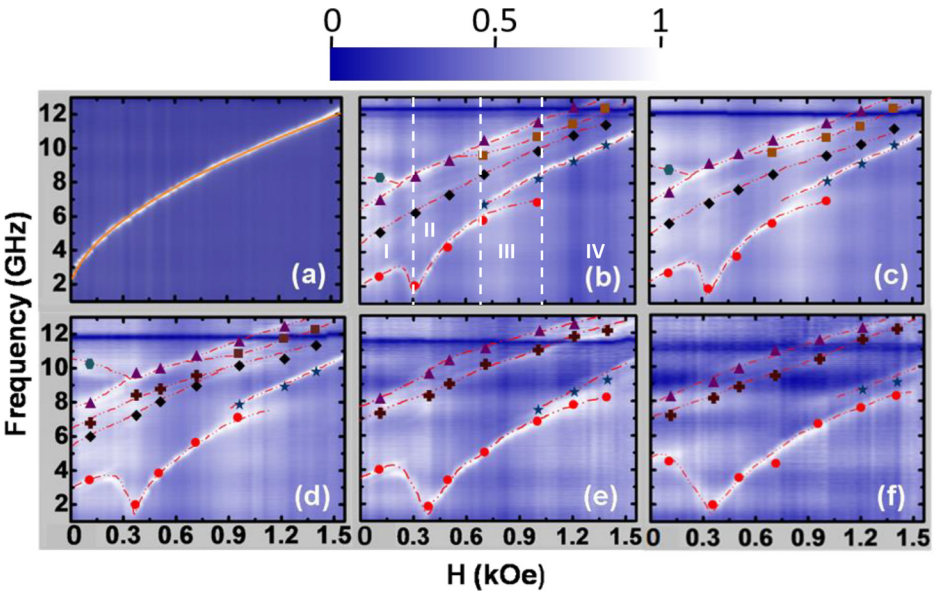

FIG. 2. Surface plots of bias field dependent SW mode frequencies for (a) $Ni_{80}Fe_{20}$ thin film of 20 nm thickness and nano-cross arrays with arm length (L) of (b) 600 nm, (c) 500 nm, (d) 400 nm, (e) 300 nm, and (f) 200 nm. The Kittel fit to (a) is shown by the solid line. Simulated SW frequencies are shown by filled symbols, while the dotted lines are guide to the eye. The color map is shown at the top of the figure.

form a single mode for an intermediate range of bias field, which is again split into two modes at a lower magnetic field and the splitting amplitude increases steeply with further reduction of the bias field value. With the variation of nano-cross dimensions, the features (a) and (b) remained qualitatively similar, while some quantitative variations occur. With the reduction in the arm length (L) of the nano-cross, the cross-over field and the field at which the minimum occurs both increase monotonically, while the field at which the maximum occurs decreases monotonically for feature (a). For feature (b), both the frequency values and the rate of variation of frequency with bias field increase with the reduction of arm length, L. For feature (c), however, a qualitative change also occurs in addition to the quantitative variation. With the reduction in arm length (L), both the fields at which the two frequency branches merge and then split again increase monotonically, while for $L \leq 300$ nm, both these features disappear and a single branch with frequency reducing monotonically with the bias field is observed.

To understand the experimental results, we performed micromagnetic simulations using OOMMF software.[28] The simulated arrays were mimicked from the SEM images and two-dimensional periodic boundary condition was applied for considering large areas of the arrays studied experimentally. The arrays were discretized into a number of rectangular prism-like cells with dimensions $4 \times 4 \times 20\,\text{nm}^3$. The material parameters, γ, M_S, and H_K, used in the simulations were extracted from the Kittel fit of the bias field dependent frequency of the Py thin film as discussed earlier, while the exchange stiffness constant $A_{ex} = 1.3 \times 10^{-6}$ erg/cm is taken from literature.[29] The damping constant of 0.008 is used during dynamic simulations, while the detailed methods of simulations are described elsewhere.[21] Figures 2(b)–2(f) show the simulated results (filled symbols), which reproduced the experimental results very well. Figure 3 shows some representative simulated SW spectra for the nano-cross with $L = 600$ nm at different bias fields, the peak values of which are plotted as symbols in Fig. 2. The simulated static magnetic configurations at four different bias fields and for nano-cross with two different arm lengths (L) are shown in Fig. 4. It is clear that the onion magnetization ground state becomes more stable for the sample with $L = 200$ nm as compared to that for the sample with $L = 600$ nm. We further simulated the power and phase profiles of the SW modes using a home-built code,[30] and Fig. 5 shows the phase profiles of the nano-cross array with $L = 600$ nm at four different bias fields. The power profiles of the same are shown in the supplementary figure (Fig. 1S). The simulated magnetic hysteresis loops of three nano-cross arrays ($L = 600$, 400, and 200 nm) are also shown in the supplementary material (Fig. 2S).

We have divided the whole range of the bias field dependence of frequency into four significant regimes. Regime-I ranges from $H = 0$ to the minimum of the lowest frequency branch. The static magnetic configuration shows formation of an S-state in this regime, which switches to an

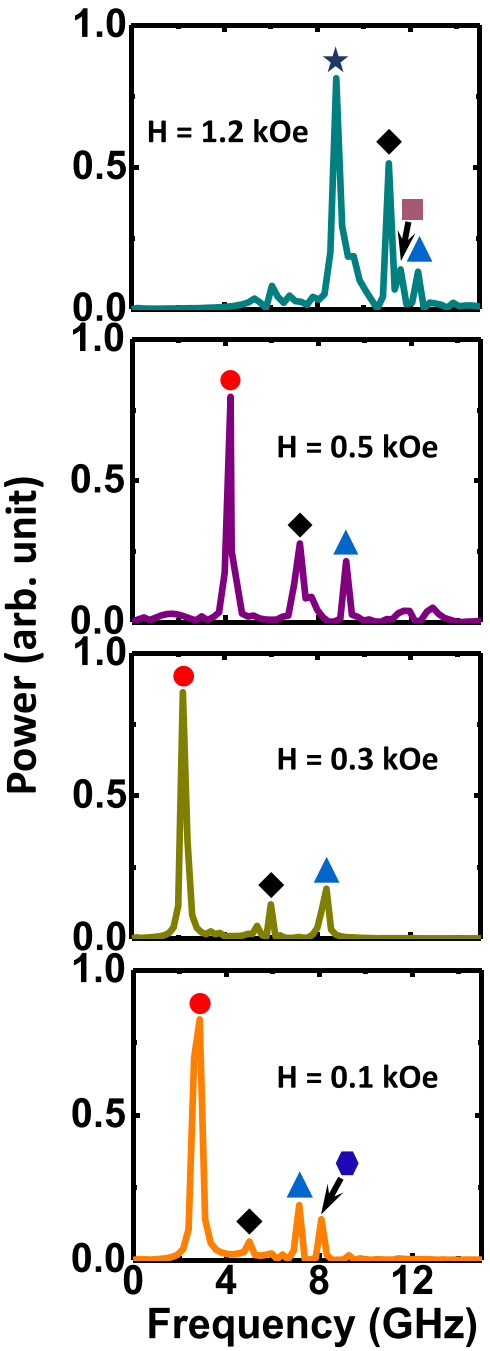

FIG. 3. Simulated spin wave spectra of the $Ni_{80}Fe_{20}$ nano-cross array with arm length (L) = 600 nm at four different bias field values. Filled colored symbols represent different SW modes.

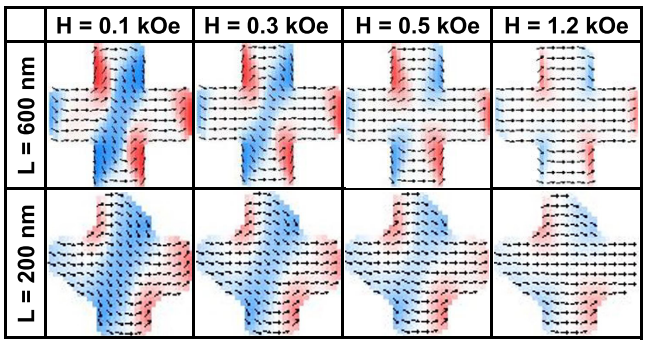

FIG. 4. Simulated static magnetic configurations for $Ni_{80}Fe_{20}$ nano-cross samples with arm lengths (L) of 600 nm and 200 nm at four different bias field values.

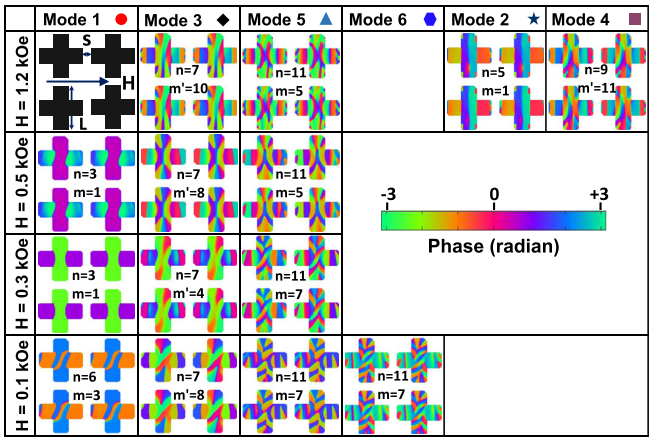

FIG. 5. Simulated spatial distribution of phase profiles corresponding to different SW modes at four different bias field values for the $Ni_{80}Fe_{20}$ nano-cross with L = 600 nm. The applied field direction is shown at the top left image. Symbols with different colors represent different SW modes. The color map is shown in the right side of the figure.

onion-state at the centre of the cross in regime-II (Fig. 4). The static magnetic configuration shows that it remains qualitatively similar for further increase in field but the spins become increasingly parallel to the bias field, which weakens the onion-state. This has a strong effect on the SW modes and mode 1 is particularly affected. In regime-I, mode 1 shows a mixed backward volume (BV; n) and Damon Eshbach (DE; m) like character with mode quantization numbers $n = 6$, $m = 3$. The sudden switching of the magnetic configuration to the onion-state causes a mode softening[31,32] and quantization numbers for mode 1 becomes $n = 3$, $m = 1$ and it remains like that as long as this mode exists. At H = 0.8 kOe, a crossover from mode 1 to mode 2 occurs (regime-III), with mode 2 showing primarily a BV-like character with $n = 5$, $m = 1$ (regime-IV). Mode 3, on the other hand, shows an azimuthal character (m') instead of the DE-like character in the vertical arm of the cross.[33] In regime-I, mode 3 is characterized by $n = 7$, $m' = 8$. However, at H = 0.3 kOe, where a minimum in mode 1 is observed, mode 3 becomes $n = 7$, $m' = 4$, possibly due to mode softening. In regime-II, mode 3 again shows $n = 7$, $m' = 8$. However, beyond the crossover (regime-IV), it becomes $n = 7$, $m' = 10$. The highest frequency mode shows a mode splitting for $H \leq 0.225$ kOe, with opposite slopes in the variation with bias field and the mode profiles for both modes (mode 5 and mode 6) correspond to $n = 11$, $m = 7$ but with opposite phases. The bias field variation with two opposite slopes of these two modes probably stems from a competition between the spin configurations in the two orthogonal arms of the nano-cross, which increases with the reduction in the bias field. For $0.225\ \text{kOe} \leq H \leq 0.62$ kOe, this mode remains as a single mode but it splits again for $H \geq 0.62$ kOe, with the appearance of a new mode (mode 4) with $n = 9$, $m' = 11$. Although we characterize mode 5 and mode 6 as mixed BV-DE mode, they still have partial azimuthal character, while mode 4 is primarily azimuthal in nature. Another interesting transition occurs for L = 400 nm where mode 3 shows a branching for $H \leq 0.88$ kOe, and this new mode shows a mixture of BV and azimuthal characters (see supplementary Fig. 3S). For L > 400 nm, mode 3 and mode 5 show no branching with almost monotonic variation with bias field. The power profiles of the modes, as shown in Fig. 1S, show the regions in the cross structures where the above modes are concentrated. The simulated hysteresis loops reveal the transition between different static magnetic configurations and the corresponding field values (Fig. 2S). The variation of the transition fields with the arm length in the static magnetic configurations of the cross structures is reflected in the variation of field values at which various important features in the dynamics occurs.

To understand the dynamics further, we have numerically calculated the magnetostatic field distributions in the nano-cross arrays, and the corresponding contour plots are shown in Fig. 6(a) for three different sizes of the nano-cross. Since the bias field is applied along the x-axis, free magnetic poles, the ensuing magnetic stray fields and demagnetizing fields are created in both horizontal and vertical arms along that direction. Line scans of the fields along the dashed lines are presented in the lower panels of Fig. 6(b), which reveal two important features. With the decrease in arm length (L), the inter-cross interaction fields as well the internal fields decrease monotonically as plotted in Figures 6(c) and 6(d). In particular, reduction in internal field is observed near the horizontal edges and at the centre of the cross with the reduction in L. This feature is probably responsible for shifting of the observed minima and a crossover of mode 1 to higher field values. On the other hand, having reasonably smaller values of inter-cross interaction fields, particularly for the smaller sizes of the nano-cross structures, ensures observation of

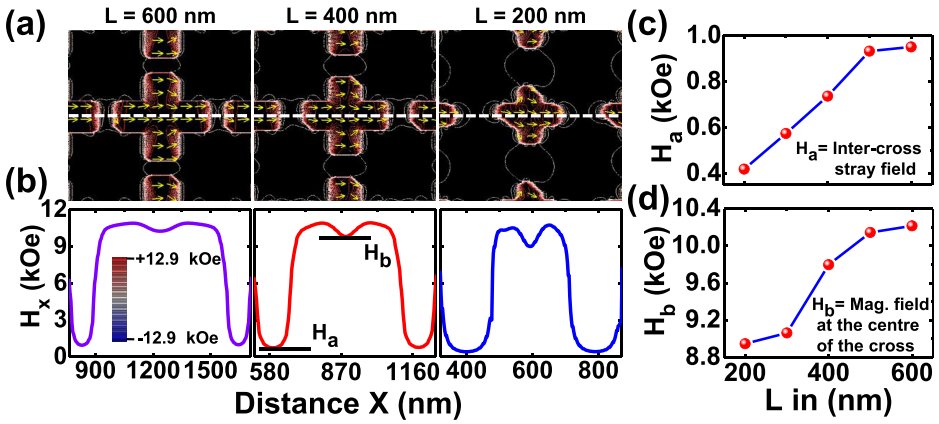

FIG. 6. (a) Contour plots of the simulated magnetostatic field distribution in $Ni_{80}Fe_{20}$ nano-cross arrays with different arm lengths (L) for H = 0.6 kOe. Line scans are taken along the white dotted lines. (b) Line scans of the simulated magnetostatic fields. The color map is shown in the inset of bottom left of the figure. (c) Inter-cross stray field and (d) effective magnetic field at the centre of the nano-cross for different arm lengths.

intrinsic modes of those nano-cross structures without any significant collective effects from the arrays.

IV. CONCLUSIONS

In summary, we investigated a bias field dependent evolution of static magnetic configuration and magnetization dynamics in $Ni_{80}Fe_{20}$ nano-cross arrays of varying sizes using the broadband ferromagnetic resonance technique. The static magnetic configuration undergoes a transition from the S-state to the onion-state with the increase in the in-plane bias field and the spins further straighten towards the bias field direction with a subsequent increase in its magnitude. Consequently, the SW modes show interesting variation. The lowest SW mode shows an increase in frequency with the initial increase in bias field, followed by a maximum, a minimum, subsequent increase in frequency, and then a crossover to a higher frequency mode. The third mode shows a monotonic increase with bias field, while the higher frequency modes again show a non-monotonic behavior. Two branches of modes merge to form a single mode, which again splits into two modes with the increase in bias field. Simulated SW mode profiles show two different types of modes, a mixed BV-DE like mode and another BV like mode mixed with azimuthal modes. Mode softening occurs when the static magnetic configuration switches from the S-state to the onion state and the crossover is found to occur between modes with different quantization numbers. With the variation of the nano-cross dimension both quantitative and qualitative variations of the dynamics occur. Calculated magnetostatic field distributions indicate the origin of the variation in the mode frequencies and mode structures and the weak inter-cross stray magnetic fields confirm nearly intrinsic nature of the dynamics of the cross without any significant collective effects from the array, particularly for the smaller nano-cross structures. The large tunability of the rich SW mode structures with the external bias field and the dimension of the cross structure offer new building blocks for magnetic storage, memory, logic, and communication devices.

SUPPLEMENTARY MATERIAL

See supplementary material for (a) power profiles of SW modes for $L = 600$ nm, (b) simulated hysteresis loops and static spin configurations for different L and at four different H, and (c) power and phase profiles of new branching mode for $L = 400$ nm at lower bias field values.

ACKNOWLEDGMENTS

The authors gratefully acknowledge the financial support from the Department of Science and Technology, Government of India under Grant No. SR/NM/NS-09/2011(G) and S. N. Bose National Centre for Basic Sciences, India (Grant No. SNB/AB/12-13/96). K.A. acknowledges UGC for Junior Research Fellowship and S.C. acknowledges S. N. Bose National Centre for Basic Sciences for Senior Research Fellowship.

[1]R. Skomskii, J. Phys.: Condens. Matter **15**, R841 (2003).
[2]S. D. Bader, Rev. Mod. Phys. **78**, 1 (2006).
[3]N. Eibagi, J. J. Kan, F. E. Spada, and E. E. Fullerton, IEEE Magn. Lett. **3**, 4500204 (2012).
[4]A. Imre, G. Csaba, L. Ji, A. Orlov, G. H. Bernstein, and W. Porod, Science **311**, 205 (2006).
[5]A. Haldar, D. Kumar, and A. O. Adeyeye, Nat. Nanotechnol. **11**, 437 (2016).
[6]V. E. Demidov, S. Urazhdin, A. Zholud, A. V. Sadovnikov, and S. O. Demokritov, Appl. Phys. Lett. **106**, 022403 (2015).
[7]S. K. Kim, K. S. Lee, and D. S. Han, Appl. Phys. Lett. **95**, 082507 (2009).
[8]Y. Au, M. Dvornik, O. Dmytriiev, and V. V. Kruglyak, Appl. Phys. Lett. **100**, 172408 (2012).
[9]S. Kaka, M. R. Pufall, W. H. Rippard, T. J. Silva, S. E. Russek, and J. A. Katine, Nature **437**, 389 (2005).
[10]M. Krawczyk and D. Grundler, J. Phys.: Condens. Matter **26**, 123202 (2014).
[11]B. Lenk, H. Ulrichs, F. Garbs, and M. Münzenberg, Phys. Rep. **507**, 107 (2011).
[12]A. V. Chumak, V. I. Vasyuchka, A. A. Serga, and B. Hillebrands, Nat. Phys. **11**, 453 (2015).
[13]A. Barman, S. Wang, J. D. Maas, A. R. Hawkins, S. Kwon, A. Liddle, J. Bokor, and H. Schmidt, Nano Lett. **6**, 2939 (2006).
[14]Z. Liu, R. D. Sydora, and M. R. Freeman, Phys. Rev. B **77**, 174410 (2008).
[15]P. S. Keatley, P. Gangmei, M. Dvornik, R. J. Hicken, J. Childress, and J. A. Katine, Appl. Phys. Lett. **98**, 082506 (2011).
[16]S. Jung, B. Watkins, L. DeLong, J. B. Ketterson, and V. Chandrasekhar, Phys. Rev. B **66**, 132401 (2002).
[17]G. Gubbiotti, G. Carlotti, T. Okuno, M. Grimsditch, L. Giovannini, F. Montoncello, and F. Nizzoli, Phys. Rev. B **72**, 184419 (2005).
[18]V. V. Kruglyak, A. Barman, R. J. Hicken, J. R. Childress, and J. A. Katine, J. Appl. Phys. **97**, 10A706 (2005).
[19]J. M. Shaw, T. J. Silva, M. L. Schneider, and R. D. McMichael, Phys. Rev. B **79**, 184404 (2009).
[20]V. V. Kruglyak, P. S. Keatley, A. Neudert, R. J. Hicken, J. R. Childress, and J. A. Katine, Phys. Rev. Lett. **104**, 027201 (2010).
[21]B. Rana, D. Kumar, S. Barman, S. Pal, Y. Fukuma, Y. Otani, and A. Barman, ACS Nano **5**, 9559 (2011).
[22]B. K. Mahato, B. Rana, D. Kumar, S. Barman, S. Sugimoto, Y. Otani, and A. Barman, Appl. Phys. Lett. **105**, 012406 (2014).
[23]S. Saha, R. Mandal, S. Barman, D. Kumar, B. Rana, Y. Fukuma, S. Sugimoto, Y. Otani, and A. Barman, Adv. Funct. Mater. **23**, 2378 (2013).
[24]K. Machida, T. Tezuka, T. Yamamoto, T. Ishibashi, Y. Morishita, A. Koukitu, and K. Sato, J. Magn. Magn. Mater. **290**, 779 (2005).
[25]B. K. Mahato, B. Rana, R. Mandal, D. Kumar, S. Barman, Y. Fukuma, Y. Otani, and A. Barman, Appl. Phys. Lett. **102**, 192402 (2013).
[26]K. Nanayakkara, A. P. Jacob, and A. Kozhanov, J. Appl. Phys. **118**, 163904 (2015).
[27]B. K. Mahato, S. Choudhury, R. Mandal, S. Barman, Y. Otani, and A. Barman, J. Appl. Phys. **117**, 213909 (2015).
[28]M. Donahue and D. G. Porter, OOMMF User's Guide, Version 1.0, NIST Interagency Report No. 6376, National Institute of Standard and Technology, Gaithersburg, MD, 1999.
[29]K. H. J. Buschow, *Handbook of Magnetic Materials* (North Holland, Amsterdam, The Netherlands, 2009).
[30]D. Kumar, O. Dmytriiev, S. Ponraj, and A. Barman, J. Phys. D: Appl. Phys. **45**, 015001 (2012).
[31]F. Montoncello, L. Giovannini, F. Nizzoli, P. Vavassori, M. Grimsditch, T. Ono, G. Gubbiotti, S. Tacchi, and G. Carlotti, Phys. Rev. B **76**, 024426 (2007).
[32]G. F. Zhang, Z. X. Li, X. G. Wang, Y. Z. Nie, and G. H. Guo, J. Magn. Magn. Mater. **385**, 402 (2015).
[33]A. A. Awad, K. Y. Guslienko, J. F. Sierra, G. N. Kakazei, V. Metlushko, and F. G. Aliev, Appl. Phys. Lett. **96**, 012503 (2010).